Monthly Notices
of the
ROYAL ASTRONOMICAL SOCIETY

MNRAS **445,** 869–880 (2014) doi:10.1093/mnras/stu1783

X-ray observations of VY Scl-type nova-like binaries in the high and low state

P. Zemko,[1⋆] M. Orio,[2,3] K. Mukai[4,5] and S. Shugarov[6,7]

[1]*Department of Physics and Astronomy, Università di Padova, vicolo dell' Osservatorio 3, I-35122 Padova, Italy*
[2]*INAF – Osservatorio di Padova, vicolo dell' Osservatorio 5, I-35122 Padova, Italy*
[3]*Department of Astronomy, University of Wisconsin, 475 N. Charter St, Madison, WI 53704, USA*
[4]*CRESST and X-ray Astrophysics Laboratory, NASA Goddard Space Flight Center, Greenbelt, MD 20771, USA*
[5]*Department of Physics, University of Maryland, Baltimore County, 1000 Hilltop Circle, Baltimore, MD 21250, USA*
[6]*Sternberg Astronomical Institute, Moscow University, Universitetsky Ave, 13, Moscow 119992, Russia*
[7]*Astronomical Institute of the Slovak Academy of Sciences, Tatranská Lomnica 059 60, The Slovak Republic*

Accepted 2014 August 27. Received 2014 August 27; in original form 2014 June 16

ABSTRACT

Four VY Scl-type nova-like systems were observed in X-rays during both the low- and the high-optical states. We examined *Chandra*, *ROSAT*, *Swift* and *Suzaku* archival observations of BZ Cam, MV Lyr, TT Ari and V794 Aql. The X-ray flux of BZ Cam is higher during the low state, but there is no supersoft X-ray source (SSS) as hypothesized in previous articles. No SSS was detected in the low state of the any of the other systems, with the X-ray flux decreasing by a factor between 2 and 50. The best fit to the *Swift* X-ray spectra is obtained with a multicomponent model of plasma in collisional ionization equilibrium. The high-state high-resolution spectra of TT Ari taken with *Chandra* Advanced CCD Imaging Spectrometer (ACIS-S) and the *Chandra* High Energy Transmission Grating (HETG) shows a rich emission line spectrum, with prominent lines of Mg, Si, Ne and S. The complexity of this spectrum seems to have origin in more than one region, or more than one single physical mechanism. While several emission lines are consistent with a cooling flow in an accretion stream, there is at least an additional component. We discuss the origin of this component, which is probably arising in a wind from the system. We also examine the possibility that the VY Scl systems may be intermediate polars, and that while the boundary layer of the accretion disc emits only in the extreme ultraviolet, part of the X-ray flux may be due to magnetically driven accretion.

Key words: accretion, accretion discs – novae, cataclysmic variables – X-rays: binaries.

1 INTRODUCTION

Nova-like (NL) stars are non-eruptive cataclysmic variables (CVs, see Warner 1995), classified into several subtypes depending on evidence of a strong magnetic field on the white dwarf (WD), and on spectral and photometric characteristics (see Dhillon 1996). Here, we will focus on the VY Scl-type NLs or 'antidwarf' novae characterized by the presence of occasional dips on the light curve, so-called low states, defined by Honeycutt & Kafka (2004) as a fading of the optical light by more than 1.5 mag in less than 150 d. The drop in luminosity can reach 7 mag and may last from weeks to years.

The large optical and UV luminosity seems to imply that the VY Scl-type NL, in their longer lasting optically high state, are undergoing mass transfer on to the WD at the high rate $\dot{m} > 10^{-10}$ $M_\odot$ yr^{-1}, sustaining an accretion disc in a stable hot state in which dwarf novae (DN) outbursts are suppressed (see e.g. the disc thermal instability model of Osaki 2005). The low states have been attributed to a sudden drop of $\dot{m}$ from the secondary, or even to a total cessation of mass transfer (see e.g. King & Cannizzo 1998; Hessman 2000). The reason of this dramatic decrease of $\dot{m}$ is still unclear. The most probable cause may be spots on the surface of the secondary, covering the L1 point and causing the mass-transfer cut-off (Livio & Pringle 1994). Wu, Wickramasinghe & Warner (1995) have suggested instead non-equilibrium effects in the irradiated atmosphere of the donor.

If the transition from the high to low state occurs because of a decrease in $\dot{m}$, the accretion discs in these systems should move from the equilibrium region to the one of DN instabilities, so we should observe (DN) outbursts with recurrence times of 12–20 d during the low state, caused by thermal–viscous instabilities in the accretion disc (Warner 1995). However, outbursts in the low state of these objects are extremely rare (see Pavlenko & Shugarov 1999, for MV Lyr). DN outbursts must be suppressed during the low state despite the low $\dot{m}$; this can be explained by a WD effective

⋆ E-mail: polina.zemko@studenti.unipd.it

Table 1. Binary parameters.

	BZ Cam	MV Lyr	TT Ari	V794 Aql
Dist(pc)	$830 \pm 160^{[1]}$	$505 \pm 50^{[3]}$	$335 \pm 50^{[7]}$	$690 \pm 105^{[10]}$
$P_{\rm orb}(d)$	$0.1536^{[2]}$	$0.1329^{[4]}$	$0.1375^{[8]}$	$0.1533^{[11]}$
$i^{\rm o}$	$12–40^{[1]}$	$10–13^{[4]}$	$17–22^{[9]}$	$60^{[10]}$
$M_{\rm WD}(M_\odot)$		$0.7 \pm 0.1^{[3]}_{\rm (FUV)}$	$0.57–1.2^{[9]}_{\rm (Opt)}$	$0.88 \pm 0.39^{[10]}$
$\dot{m}_{\rm High}(M_\odot\ {\rm yr}^{-1})$		$2–3\times 10^{-9}{}_{\rm (FUV,\ Opt)}{}^{[5],\,[6]}$	$1.1 \times 10^{-8}{}_{\rm (Opt)}{}^{[9]}$	$10^{-8.5}–10^{-8.0}{}_{\rm (FUV)}{}^{[10]}$
$\dot{m}_{\rm Low}(M_\odot\ {\rm yr}^{-1})$		$3\times 10^{-13}{}_{\rm (Opt)}{}^{[3]}$	$10^{-16}–10^{-15}{}_{\rm (UV)}{}^{[7]}$	
$T_{\rm WD\,High}$		$\geq 50\,000\ {\rm K}^{[5]}_{\rm (FUV)}$		
$T_{\rm WD\,Low}$		$47\,000\ {\rm K}^{[3]}_{\rm (FUV)}$	$39\,000\ {\rm K}^{[7]}_{\rm (UV)}$	$45\,000\ {\rm K}^{[10]}_{\rm (FUV)}$
$T_{\rm Disc\,Low}$		$< 2500\ {\rm K}^{[6]}_{\rm (UV)}$		
FUV $\rm Flux_{High}$(erg cm^{-2} s^{-1})		$1.4\times 10^{-10}{}^{[5]}\star$	$7.8 \times 10^{-10}{}^{[12]}\star\star$	
FUV $\rm Flux_{Low}$ (erg cm^{-2} s^{-1})		$9.4\times 10^{-12}{}^{[3]}\star\star$		

Notes. (FUV), (UV), (Opt) – values obtained from FUV, UV and Optical observations, respectively. $\star$ FUV flux was evaluated from the mean continuum level of a spectrum in a range 910–1190 Å.
$\star\star$FUV flux was evaluated from the mean continuum level of a spectrum in a range 920–1180 Å.
[1] Ringwald & Naylor (1998), [2] Patterson et al. (1996), [3] Hoard et al. (2004), [4] Skillman, Patterson & Thorstensen (1995), [5] Godon & Sion (2011), [6] Linnell et al. (2005), [7] Gänsicke et al. (1999), [8] Thorstensen, Smak & Hessman (1985), [9] Belyakov et al. (2010), [10] Godon et al. (2007), [11] Honeycutt & Robertson (1998), [12] Hutchings & Cowley (2007).

temperature high enough (30 000–50 000 K) to irradiate the inner accretion disc and maintain it in the stable 'hot' state (Smak 1983), while the incoming mass accretion stream stops or decreases (King 1997; Hameury, Lasota & Dubus 1999; Lasota 1999; Leach et al. 1999). The WD in the known DN never reaches this temperature range, but high WD effective temperatures have indeed been inferred via spectroscopic observations in the ultraviolet UV and far-ultraviolet (FUV) ranges for the VY Scl objects (see Table 1). Hameury & Lasota (2002) suggested instead that the DN outbursts are prevented by the periodic disruption of the disc by a magnetic field of the WD, and in this model the VY Scl would be intermediate polars (IPs), in which the WD magnetic field is of the order of 10^6 G.

Greiner et al. (1999) proposed a link between the VY Scl-type stars and supersoft X-ray sources (SSSs) based on a *ROSAT* observations of V751 Cyg. They found an anticorrelation in the optical and X-ray intensity, and despite the very poor spectral resolution of the *ROSAT* high resolution imager (HRI), the spectrum appeared to be soft in the low state. The authors suggested that quasi-stable thermonuclear burning occurs on the surface of the WD in the low state, preventing DN outbursts. In this framework, VY Scl stars are key objects in the evolution of interacting WD binaries, in which hydrogen burning occurs periodically without outbursts. Accretion goes on at a very high rate without ever triggering a thermonuclear runaway, because of the recurrent interruptions of the high $\dot{m}$ regime. Thus, there is a possibility that VY Scl stars reach the Chandrasekhar mass and the conditions for Type Ia supernovae outbursts. Greiner & Teeseling (1998) and Greiner et al. (2001) suggested also thermonuclear burning in the low states of V Sge and BZ Cam. However, these two objects had not been actually observed as SSS; in more recent years an X-ray observation of the VY Scl system V504 Cyg in the low state failed to reveal a luminous SSS (Greiner et al. 2010).

Using archival X-ray observations, in this paper, we compare high- and low-state X-ray data, and some new *UV* data, for four VY Scl-type stars. We seek clues to the complex evolution of these systems, and explanations for the changes that take place during the transition from the high to low state.

2 PREVIOUS OPTICAL AND UV OBSERVATIONS

In Table 1, we report parameters from the published results of observations in the optical, NUV and FUV wavelength ranges. We see that these objects have an orbital period just above the period gap, in a narrow range between 3.2 and 3.7 h. For the three systems MV Lyr, TT Ari and V794 Aql the WD effective temperature $T_{\rm eff}$ was estimated in previous low states (not shown in Fig. 1) from UV and FUV observations, in the range between 39 000 and 47 000 K. These systems could not have been SSS at the time of those observations, because $T_{\rm eff}$ places the flux peak in the FUV range. On the other hand, we cannot rule out ignition of thermonuclear burning, neither the possibility that the WD may become hotter with time in subsequent low states. The low state $T_{\rm eff}$ of MV Lyr tabulated in Table 1 was measured while the FUV flux, corresponding to most of the bolometric one, was about 3.6×10^{-12} erg s^{-1} (see Table 1). In fig. 5 of Starrfield et al. (2012), we see that at the tabulated distance these values may be consistent with thermonuclear burning with $\dot{m} < 1.6 \times 10^{-10}\ {\rm M}_\odot\ {\rm yr}^{-1}$ and a WD mass less than 1 $M_\odot$. Godon & Sion (2011) suggested that MV Lyr becomes hotter in the high state, hypothesizing a lower limit $T_{\rm eff} \geq 50\,000$ K, consistent with a measured FUV flux of 2.5×10^{-10} erg s^{-1} in the high state. If the WD really becomes hotter while emitting X-rays at this level, the possibility of thermonuclear burning would be even more likely in the high state. For a WD mass of 0.7 $M_\odot$ and the value of $\dot{m}$ in Table 1, assuming that the extreme UV (EUV) luminosity is close to the total (bolometric) luminosity, nuclear burning according to Starrfield et al. (2012) occurs with $T_{\rm eff} \simeq 80\,000$ K (see their fig. 5), which implies a peak luminosity in the EUV range and no detectable SSS. An accurate determination of $T_{\rm eff}$ in the high state is important: even an upper limit inferred from the absence of an SSS in the X-rays is useful to constrain the evolutionary models.

3 OBSERVATIONS AND DATA ANALYSIS

We examined the archival X-ray data of VY Scl-type stars obtained with *Swift*, *ROSAT*, *Suzaku* and *Chandra* and chose the objects that

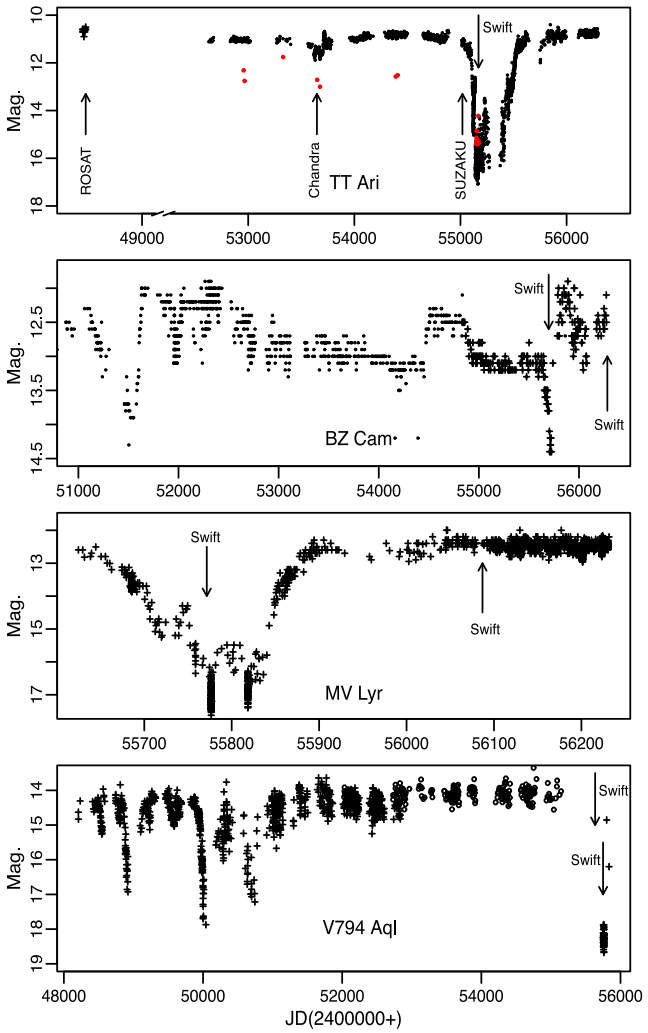

Figure 1. Light curves of TT Ari, BZ Cam, MV Lyr and V794 Aql (from top to bottom) obtained from the AAVSO (crosses), VSNET (filled circles) collaboration and ASAS (open circles) data. The times of the X-ray observations are marked with arrows.

were observed both in the high and low states: BZ Cam, MV Lyr, TT Ari and V794 Aql. The data are summarized in Table 2. All the data were never published except for a *ROSAT* observations of TT Ari, which we examined again and which were also analysed by Baykal et al. (1995) and van Teeseling, Beuermann & Verbunt (1996).

In order to assess when the low- and high-optical states occurred, we relied on the data of the Variable Star Network (VSNET) Collaboration (Kato et al. 2004),[1] the American Association of Variable Star Observers (AAVSO)[2] and ASAS (Pojmanski 1997)[3] data bases. The optical light curves are presented in Fig. 1. The epoch of the X-ray observation is marked with an arrow in each plot. We did not find optical data for V794 Aql around the epoch of the X-ray observations taken on 2011 March 15. However, from the photometric observations of the object before and after this date presented in Honeycutt et al. (2014), it is reasonable to assume that V794 Aql was in the intermediate state during the X-ray observation.

[1] http://www.kusastro.kyoto-u.ac.jp/vsnet/
[2] http://www.aavso.org
[3] http://www.astrouw.edu.pl/asas/

We used the HEASOFT version 6–13 to extract the *Swift* and *Suzaku* spectra, and the XSPEC version 12.8.0 for spectral modelling. We also measured the UV magnitudes of the objects in both the *Swift*/UltraViolet and Optical Telescope (UVOT) observations and in additional *GALEX* archival exposures. The *Chandra* Advanced CCD Imaging Spectrometer (ACIS-S)+HETG grating spectra were extracted with CIAO version 4.3. Four different partial exposures were added for both the high energy grating (HEG) and medium energy grating (MEG) spectra with the FTOOL ADDASCASPEC, written originally for *ASCA*, but also useful for all X-ray telescopes and detectors.

For better resolution and in order to use the full exposure, we also combined the data from two *Suzaku* front illuminated detectors (XIS 0 and XIS 3) taken in 3×3 and 5×5 modes. The timing analysis of the *Suzaku* data was performed with the XRONOS sub-package of FTOOLS after the barycentric correction.

4 RESULTS

4.1 TT Ari

TT Arietis is one of the brightest CVs, usually between *V* magnitude 10 and 11. Sometimes it abruptly falls into an 'intermediate state' at $V \simeq 14$ or even into a 'low state' reaching $V \simeq 18$. According to Belyakov et al. (2010) this binary system consists of a 0.57–1.2 $M_\odot$ WD and a 0.18–0.38 $M_\odot$ secondary component of M 3.5±0.5 spectral type (Gänsicke et al. 1999). The only low state before the one discussed in this paper was observed in the years 1980–1985 (Hudec, Huth & Fuhrmann 1984; Shafter et al. 1985). The first panel of Fig. 1 shows the long-term light-curve of TT Ari between 1990 and 2013. The optical brightness started declining dramatically at the beginning of 2009 and the low state lasted for about 9 months, with a drop in optical luminosity of about 7 mag. However, in the low state the optical luminosity is not constant, with variations between $V = 15$ and $V = 18$.

The high-state X-ray spectrum of TT Ari was at first obtained by *EXOSAT* in 1985 Aug 21/22 Hudec et al. (1987). Authors found that the X-ray flux in the range 0.2–4.0 keV was about 1.9×10^{-11} erg cm^{-2} s^{-1}. They also proposed that there are two or more hot emitting X-ray regions and two or more cold absorbing or scattering regions in TT Ari. On 1994 January 20–21, TT Ari was also observed with *ASCA* with an effective exposure time ∼14 000 s. Detailed analysis of these data was performed by Baykal & Kiziloğlu (1996). One of the most interesting findings of the previous X-ray observations is the rapid variability of the X-ray flux, a quasi-periodic oscillations (QPO) with a semiperiod of 15–26 min (Baykal et al. 1995; Baykal & Kiziloğlu 1996). We will show that QPO with periods in this range are observed in all the high-state observations we examined. In 2005, the *Chandra* HETG spectra of TT Ari were obtained by C. Mauche (first shown in a presentation by Mauche 2010). Below we will discuss this set of observations in details.

4.1.1 *The X-ray data: the high state*

A set of four *Chandra* HETG exposures were obtained within 5 weeks in 2005 (for details see Table 2). In the optical, the source was undergoing a 'shallow decline' from the average optical magnitude in the high state, from $V \simeq 10.5$ to $V \leq 11.5$. Fig. 2 shows the co-added MEG and co-added HEG spectra of four subsequent exposures. There was no significant flux or spectral variability between the different exposures, and we shall describe the co-added MEG

Table 2. Observational log of the *ROSAT*, *Swift*, *Suzaku* and *Chandra* observations of VY Scl-type NLs that were analysed in this paper.

Name	State	Date	Instrument	Exposure(s)	Count rate (cts s^{-1})
BZ Cam	High	21/12/2012	*Swift*-XRT	15 001	0.0720 ± 0.0024
	Low	15/05/2011	*Swift*-XRT	2710	0.100 ± 0.006
MV Lyr	High	08/06/2012	*Swift*-XRT	7569	0.096 ± 0.003
	Low	29/07/2011	*Swift*-XRT	3282	0.039 ± 0.004
TT Ari	High	01/08/1991	*ROSAT*-PSPCB	24464	0.098 ± 0.007
	High	06/09/2005	*Chandra*-HEG	95 362*	0.0266 ± 0.0003
	High	06/09/2005	*Chandra*-MEG	95 362*	0.0588 ± 0.0005
	High	06/07/2009	*Suzaku*-XIS FI**	28 617	0.671 ± 0.003
	High	06/07/2009	*Suzaku*-XIS BI**	28 617	0.836 ± 0.005
	Intermediate	16/10/2009	*Swift*-XRT	4421	0.278 ± 0.008
	Low	22/11/2009	*Swift*-XRT	12 030	0.0285 ± 0.0019
V794 Aql	Intermediate	15/03/2011	*Swift*-XRT	6148	0.176 ± 0.005
	Low	12/07/2011	*Swift*-XRT	4629	0.055 ± 0.003

*Four observations were taken with *Chandra*-MEG and *Chandra*-HEG on 2005 September 6 and October 4, 6 and 9.
** *Suzaku*-XIS FI – are XIS 0 and XIS 3 detectors with front-illuminated (FI) CCDs, while *Suzaku*-XIS BI is the XIS 1 that utilizes a back-illuminated (BI) CCD

and HEG spectra. A rich emission line spectrum was measured, with strong emission lines of Mg, Si, Ne and S.

The strongest lines of the *Chandra* MEG spectrum are listed in Table 3. For the H-like lines, we evaluated the flux with a Gaussian fit to the line; we also estimated the flux in the He-like triplet lines (Ne IX, Mg XI, Si XIII), but we could only do it with larger uncertainty because the lines are blended and we needed to fit three Gaussians (note that the intercombination line is not resolved). Moreover, the triplets of He-like lines are observed in a region of the spectrum which is rich in other lines, like those due to transitions of iron. Despite these difficulties, we performed the fit with three Gaussians for the triplets of Si XIII and Mg XI. We added a fourth line of Fe XVIII at 13.509 Å for Ne IX. We thus evaluated the R ratio f/i (intensity of the forbidden to the intercombination line) and the G ratio $\frac{(f+i)}{r}$ (where r is the intensity of the resonance line). We estimated an uncertainty of about 20 per cent on both these ratios. We obtained $R = 0.63$ and $G = 0.78$ for Ne IX, $R = 0.36$ and $G = 0.66$ for Mg IX, $R = 0.33$ and $G = 0.66$ for Si XIII.

We consulted Porquet & Dubau (2000), who explored the dependence of these ratios on electron density and plasma temperature. The authors assumed a photoionized plasma, with or without additional collisional ionization. We see from their fig. 8 that the R ratios we obtained corresponds to high density; we obtain a lower limit on the electron density $n_e = 10^{12}$ cm^{-3}, 10^{13} cm^{-3} and $\geq 10^{14}$ cm^{-3} for Ne, Mg and Si, respectively. However, it is known that the R ratios appears smaller, as if the density was higher than its actual value, when there is also photoexcitation by a strong UV/EUV source, exciting the f-level electrons into the i level (Porquet & Dubau 2000). We do expect additional photoexcitation if the lines are produced very close to the hot and luminous WD of TT Ari, thus, we do not know that in this case the R ratio is a completely reliable indicator. The G ratio, on the other hand, is reliable and indicates plasma temperature $\geq 3 \times 10^6$ K, $\geq 4 \times 10^6$ K and $\geq 7 \times 10^6$ for Ne, Mg and Si, respectively.

The next step was to fit the observed spectra with a physical model. A fit with a plasma in collisional ionization equilibrium is

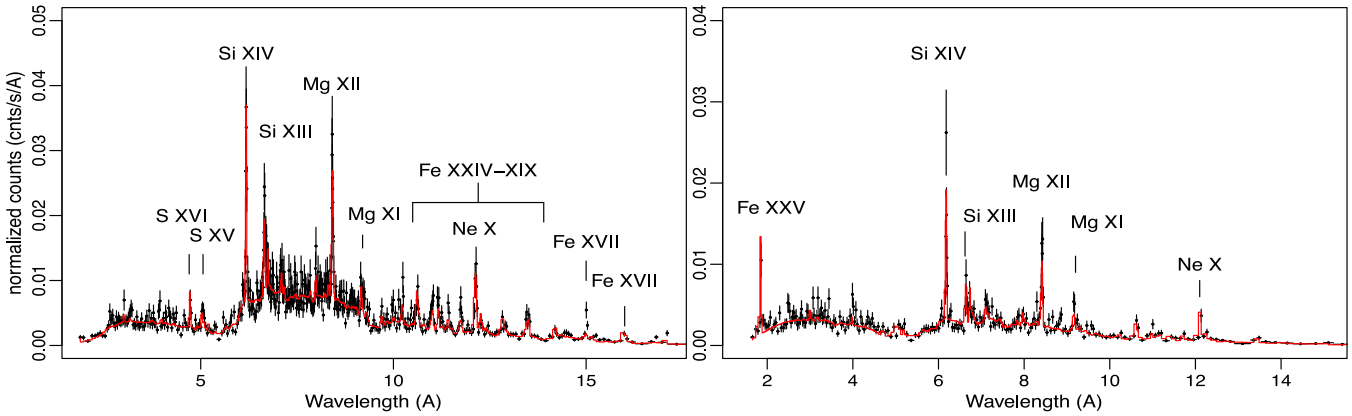

Figure 2. TT Ari spectra observed with the *Chandra* MEG (left) and HEG (right) grating. Four observations and +1 and −1 orders summed. The red lines represent the fit with two VAPEC components. The emission lines are indicated.

Table 3. Measured wavelength and fluxes in erg cm^{-2} s^{-1} $\times$ 10^{-14} for the emission lines identified in the summed *Chandra* MEG spectrum.

Element	Energy$_{obs}$ (KeV)	λ_{obs} (AA)	MEG flux$^{[1]}_{abs}$
S XV	2.4606^{r}	5.0387	2.8
	2.448^{i}	5.064	3.3
	2.4260^{f}	5.1106	3.4
Si XIV	$2.0061^{+0.0006}_{-0.0010}$	$6.1803^{+0.003}_{-0.0017}$	6.12
Si XIII	1.8650^{r}	6.6479	3.4
	1.854^{i}	6.687	1.7
	1.8396^{f}	6.6739	0.57
Mg XII	$1.4733^{+0.0003}_{-0.0011}$	$8.4154^{+0.006}_{-0.0020}$	3.07
Mg XI	1.3522^{r}	9.1687	2.0
	1.3434^{i}	9.2291	1.6
	1.3312^{f}	9.3136	0.59
Ne X	$1.0211^{+0.0007}_{-0.0004}$	$12.142^{+0.005}_{-0.008}$	5.25
Ne IX	0.9220^{r}	13.44	3.3
	0.9149^{i}	13.55	1.8
	0.9051^{f}	13.69	0.59
Fe XVIII	0.8735	14.19	0.74
Fe XVII	$0.8256^{+0.0004}_{-0.0005}$	$15.017^{+0.008}_{-0.008}$	2.98
Fe XVII	$0.7388^{+0.0006}_{-0.0005}$	$16.781^{+0.014}_{-0.013}$	4.8

[1] For a calculation of fluxes in the lines, we assumed $N(H) = 0.06 \times 10^{22}$. ^{r} – resonance, ^{i} – intercombination and ^{f} – forbidden lines.

not acceptable because of too high χ^2, but adding a second temperature we obtained a more reasonable fit, with $\chi^2 = 1.2$. We adopted two BVAPEC models in XSPEC, which describe the emission spectrum of collisionally ionized diffuse gas, calculated using the ATOMDB code v2.0.1 with variable abundances at different temperature (see Table 4 and Fig. 2) and with velocity broadening. By letting the abundances of single elements vary, we found the best fit with the following values for the abundances: [Ne/H] = 6.3 ± 1.2, [Mg/H] = 4.8 ± 0.8, [Si/H] = 4.9 ± 0.9, [S/H] = 11 ± 4, [Fe/H] = 1.46 ± 0.25, [O/H] = 10 ± 4. The emission measure of the cooler component is 3.1× 10^{53} cm^3 and the emission measure of the hotter component is 3.6 × 10^{54} cm^3. We note that, if these two regions are related to accretion, for an electron density of the order of 10^{14} cm^{-3} (the minimum electron density derived from the *G* ratio for Si), the linear dimension of the emission region is of the order of 3.1 × 10^8 and 7.1 × 10^8 cm, respectively. This is, of course, a purely phenomenological model; two large and distinct regions with different plasma temperature are difficult to explain in a physically realistic way.

BVAPEC model performs the Gaussian fitting of the lines and gives the σ for two systems of lines associated with the two components (see Table 4). The full width at half-maximum (FWHM) that corresponds to these values of σ is about 1100 and 1500 km s^{-1}.

We also wanted to try and better understand the physical scenario by adopting a more physically realistic model. Mukai et al. (2003) have shown that accretion in all non-magnetic CVs, and often even in magnetic ones, is best described by a stationary cooling flow model. We thus used the cooling flow VMCFLOW model in XSPEC (a cooling flow model after Mushotzky & Szymkowiak 1988). We see however that this fit yields a larger χ^2 value than the previous simplified model, and this is mainly because there is more flux in the He-like lines than predicted by the model. This may be due to additional photoionization, for instance in a wind from the system, implying that not all the X-ray flux is produced in the accretion flow. The main problem, however, is that the cooling flow model includes the mass accretion rate $\dot{m}$ as a parameter, but predicts a very low value for $\dot{m}$, only 3.48 × 10^{-11} $M_\odot$ yr^{-1}, while the UV and optical observations indicate 10^{-8} $M_\odot$ yr^{-1} for the high state $\dot{m}$ (see Table 1). We thus conclude that either the observed X-ray flux

Table 4. Fitting models and parameters for TT Ari. The errors represent 90 per cent confidence region for a single parameter.

		high state				low state	
Satellite	*ROSAT*	*Chandra*		*Suzaku*		*Swift*	
models	2 APEC	2 BVAPEC	VMCFLOW	2 VAPEC+GAUSS*	VMCFLOW+GAUSS*	2 APEC	APEC
$N(H)_1(10^{22})$	$0.0306^{+0.003}_{-0.0026}$	$0.048^{+0.060}_{-0.048}$	$0.026^{+0.013}_{-0.015}$	$0.136^{+0.022}_{-0.021}$	$0.075^{+0.007}_{-0.010}$	$0.04^{+0.09}_{-0.04}$	$0.019^{+0.05}_{-0.019}$
$N(H)_2(10^{22})$		$0.121^{+0.029}_{-0.029}$					
T_1 (keV)	$0.89^{+0.09}_{-0.11}$	$0.93^{+0.029}_{-0.03}$		$0.80^{+0.13}_{-0.05}$		$0.7^{+0.3}_{-0.4}$	$3.4^{+1.4}_{-0.7}$
T_2 (keV)	25^{+25}_{-13}	$6.5^{+0.5}_{-0.4}$		$7.1^{+0.3}_{-0.3}$		$3.9^{+2.7}_{-1.0}$	
Sigma$_1$ (km s^{-1})		646^{+81}_{-81}					
Sigma$_2$ (km s^{-1})		461^{+119}_{-105}					
EM$_1$ (10^{53} cm^{-3})**		$3.16^{+0.43}_{-0.26}$					
EM$_2$ (10^{53} cm^{-3})**		$36.50^{+0.10}_{-0.10}$					
T_{min} (keV)			$0.20^{+0.026}_{-0.026}$		$0.120^{+0.016}_{-0.009}$		
T_{max} (keV)			$21.6^{+1.9}_{-1.4}$		$26.9^{+1.0}_{-1.5}$		
$\dot{m}$ ($\times$ 10^{-11} $M_\odot$yr^{-1})			$3.36^{+0.27}_{-0.22}$		$5.02^{+0.17}_{-0.11}$		
Flux$^{\star\star\star}_{abs}$	$5.76^{+0.3}_{-0.13}$	$9.35^{+0.18}_{-0.27}$	$9.01^{+0.011}_{-0.3}$	$15.81^{+0.020}_{-0.020}$	$16.18^{+0.20}_{-0.3}$	$0.99^{+0.17}_{-0.18}$	$0.94^{+0.17}_{-0.18}$
Flux$^{\star\star\star}_{unabs}$	$6.70^{+0.3}_{-0.13}$	$10.35^{+0.18}_{-0.27}$	$9.21^{+0.011}_{-0.3}$	$17.39^{+0.020}_{-0.020}$	$17.19^{+0.20}_{-0.3}$	$1.08^{+0.17}_{-0.18}$	$1.03^{+0.17}_{-0.18}$
χ^2	1.0	1.2	1.6	1.0	1.2	1.0	1.2

*We added a Gaussian at 6.41 keV in order to fit the Kα iron reflection line in the *Suzaku* spectrum.

**Emission measure.

***The X-ray flux ($\times$ 10^{-12} erg cm^{-2} s^{-1}) was calculated in the following energy ranges: 0.2–2.5 keV for *ROSAT* PSPC, 0.4–10.0 keV for *Chandra* HETG, 0.5–12.0 keV for *Suzaku* XIS FI and 0.3–10.0 keV for *Swift* XRT.

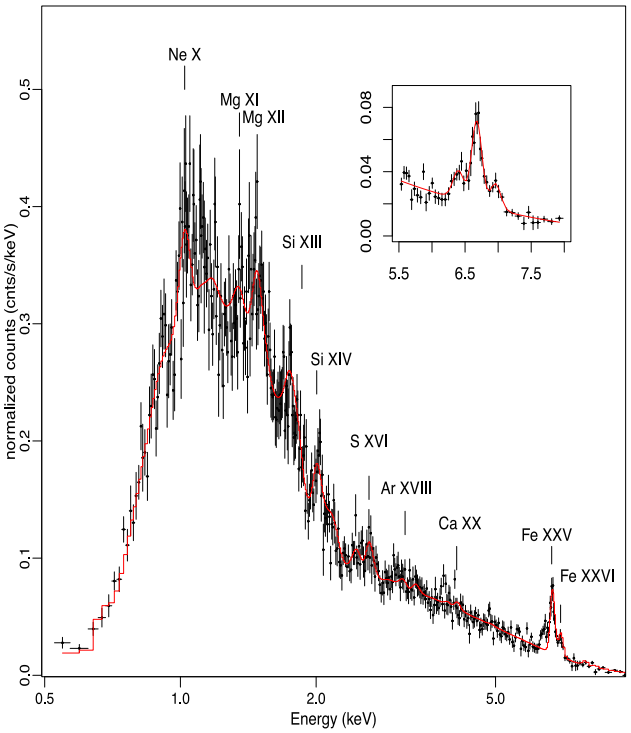

Figure 3. Spectrum observed with the *Suzaku* XIS FI (data from XIS0 and XIS3 detectors taken in 3×3 and 5×5 modes are summed). The red line shows the fit with two VAPEC components. The emission lines are indicated. The inset show the iron Kα emission lines at 6.41, 6.68 and 6.96 keV and their fit with three Gaussians.

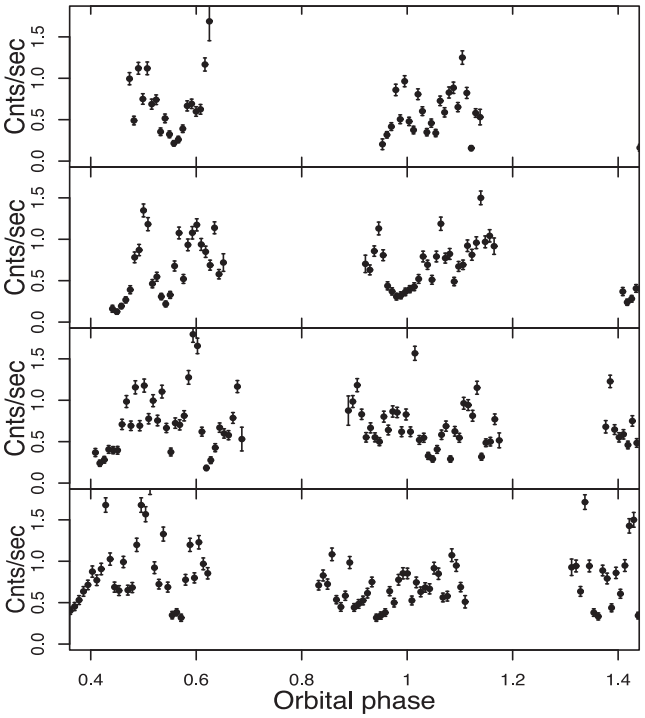

Figure 4. X-ray light curve of TT Ari, obtained by *Suzaku*, binned every 100 s. The horizontal axis is the orbital phase. The plots are in chronological order.

does not originate in the accretion flow that produces the luminous accretion disc, or that accretion energy is mostly re-radiated in the EUV and not in the X-ray range.

The light curves of these *Chandra* exposures still show a QPO, although the modulation has a $\simeq$21 min period. We discuss in detail below the similar light curve, we extracted from an additional archival observation done with *Suzaku*, which has higher S/N.

Suzaku observations of TT Ari were obtained by Saitou in 2009 just before the low state (see the top panel of Fig. 1). The average X-ray flux during this observation was higher by almost a factor of 2 than during the *Chandra* observation. In order to exclude the effect of slightly different energy ranges of the detectors, we compared the X-ray flux in the range 0.5–10.0 keV, common for both instruments. The difference between the X-ray flux measured with *Chandra* and *Suzaku* may be correlated with the optical one. The *Chandra* HETG observations were taken at the time when TT Ari was optically less luminous ($\geq$1 mag).

The broad-band spectrum of TT Ari observed with *Suzaku* is presented in Fig. 6. Emission lines of Ne, Mg and Si are clearly seen, like in the *Chandra* spectrum, together with S, Fe XXV and Fe XXVI lines. We fit this spectrum either with a two-component thermal plasma model with temperatures 0.80 and 7.1 keV (for details see Table 3) and the abundances that were derived from the *Chandra* spectra fit. The residuals of the fit indicate an extra line feature at 6.4 keV in the *Suzaku* spectrum that is most probably the iron fluorescence line. In the inset in Fig. 3, we show the fit of the 5.5–8.0 keV region with three Gaussians at 6.41, 6.68 and 6.96 keV. The equivalent width of the Kα iron line at 6.41 keV is 96^{+24}_{-24} eV. This line implies that the X-ray emission region is close to a 'cold' source, which may be the WD surface and/or an optically thick accretion disc, and it is consistent with the WD being less hot than about 100 000 K.

The cooling flow model can be used also for the *Suzaku* spectrum because we do measure spectral lines to constrain the model. The fit is not optimal, and we run into the same problem of low $\dot{m}$.

The *Suzaku* light curve is shown in Fig. 4 and is extremely similar to the light curve previously observed with *ROSAT* (Baykal et al. 1995). The data were integrated in bins of 100 s. The QPO have an amplitude of 50 per cent. In Fig. 5, we present the Fourier power spectrum of *Suzaku* light curve of TT Ari. The highest peak corresponds to 0.839 mHz or 19.8 min oscillations. According to Andronov et al. (2009) at the time of *Suzaku* observations TT Ari also showed QPO in the optical range, with several peaks, at 2.5, 1.1 and 0.38 mHz. In Baykal et al. (1995) the frequency of QPO in X-ray was explained as the beat frequency between the Kepler frequency at the inner edge of the accretion disc and the star's rotation rate. Nevertheless, from the QPO semiperiods measured by us in the *Chandra* and *Suzaku* observations and from those derived by Baykal et al. (1995) and Baykal & Kiziloğlu (1996), no correlation emerges between the observed frequency of QPO and the X-ray flux of TT Ari (see the bottom panel of Fig. 5).

In 1991, TT Ari was observed with *ROSAT*. The *ROSAT* X-ray spectrum is shown in Fig. 6. Baykal et al. (1995) analysed these data and found that the best-fitting model is an absorbed blackbody. We reanalysed the data and found that a blackbody can represent only the soft part of the spectrum (the *ROSAT* energy range is 0.2–2.4 keV) and for a more sophisticated fit we need two-component thermal plasma model. Parameters of the best-fitting model are presented in Table 4.

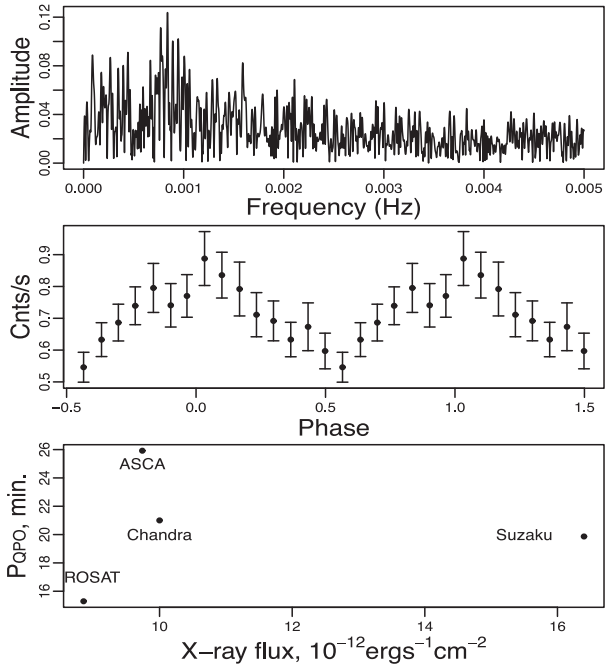

Figure 5. Top panel: the Fourier power spectrum of the *Suzaku* light curve of TT Ari. The highest peak corresponds to 0.839 mHz or 19.8 min oscillations. Middle panel: phase folded *Suzaku* light curve with 19.8 min period. Bottom panel: periods of the QPO and flux in the X-ray range 0.5–10.0 keV in the *ROSAT*, *ASCA*, *Chandra* and *Suzaku* observations. We assumed the values of Baykal & Kiziloğlu (1996) for the *ASCA* observations and for the *ROSAT* X-ray flux. The period of the QPO observed with *ROSAT* was taken from Baykal et al. (1995).

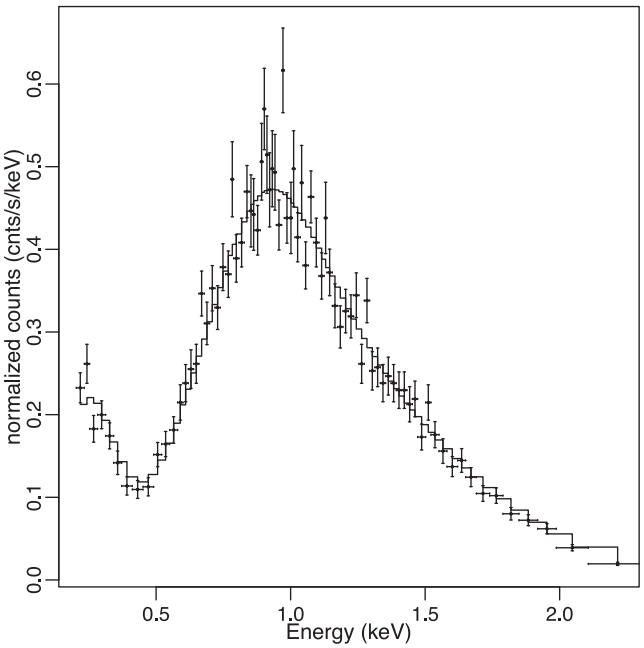

Figure 6. High-state X-ray spectrum of TT Ari taken with *ROSAT*.

4.1.2 The X-ray data: the low state

In the intermediate and low states, TT Ari was observed with *Swift*. The observations in the intermediate state were presented by Mukai et al. (2009). The unabsorbed flux was about the same as during the *Suzaku* observation, 1.5×10^{-11} erg cm^{-2} s^{-1}, the spectrum could only be fitted with a multitemperature plasma, and a new quasi-period of 0.4 d was also measured in optical.

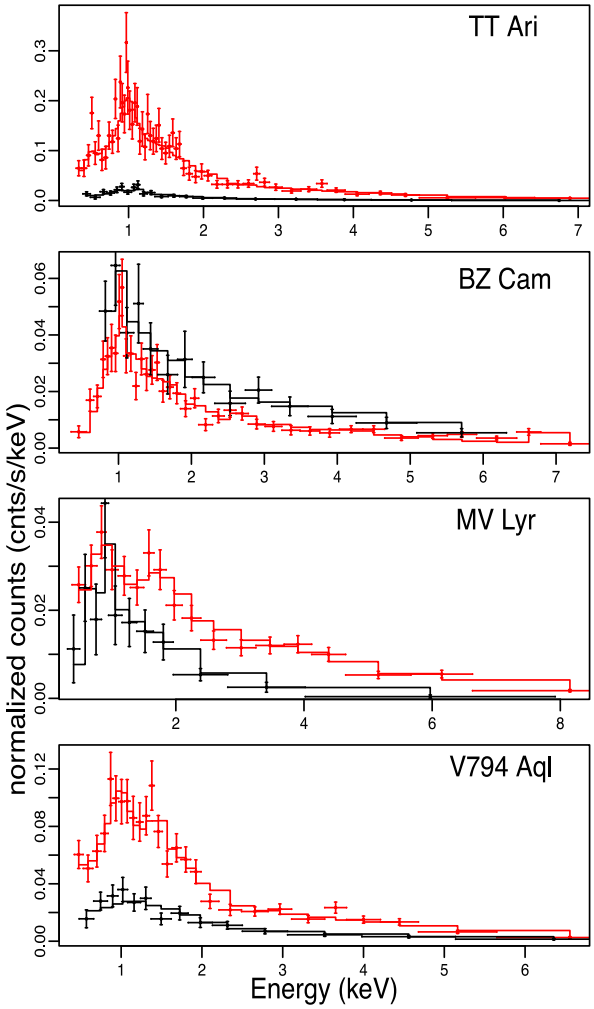

Figure 7. The low- and high-state X-ray spectra of BZ Cam and MV Lyr observed with *Swift*. TT Ari and V794 Aql were observed with *Swift* during the low and intermediate states. The high- and intermediate-state spectra are plotted in red and the low-state spectra in black. The solid lines show the models, the dots with error bars indicate the data.

The low-state spectrum, presented in the top panel of Fig. 7, is best fitted with two components of absorbed thermal plasma in collisional ionization equilibrium with a fixed metallicity APEC model at 0.7 and 3.9 keV, respectively (we only set a fixed metallicity with solar abundances because of the poorer data quality of this data set). The low-state X-ray flux appeared to be about 10 times smaller than in the high and intermediate states, and definitely no luminous supersoft X-ray phase was detected. In Table 4, we show also present the comparison with only one component at 3.4 keV. An upper limit to the temperature of a blackbody-like component is approximately 150 000 K.

4.1.3 UV data

In the first panel of Fig. 1, in addition to the optical light curve of TT Ari, the red points show the *GALEX* near UV (NUV) observations. In Table 6, we give exposure times and the mean AB magnitude in the *U*/UV filters during the low and high states. The amplitude

of the low to high-state transition in NUV was much lower than in optical: 3 versus 7 mag. Like in the optical range, TT Ari shows flaring activity in the NUV, with amplitudes up to 1 mag. However, the UV and optical flares occur at different times, and do not appear to correlated, neither anticorrelated. It may be due to the different origin of the UV and optical radiation.

4.2 BZ Cam

BZ Cam shows brightness variations around an average value $V = 12$–13, with rare occasional transitions to low states with $V = 14$–14.5. Besides the low state studied here, two additional low states were detected – in 1928 and at the beginning of 2000 (Garnavich & Szkody 1988 and Greiner et al. 2001, respectively). BZ Cam is surrounded by a bright emission nebula with a bow-shock structure, first detected by Ellis, Grayson & Bond (1984) and also studied by Krautter, Radons & Klaas (1987), Hollis et al. (1992), Greiner et al. (2001). Hollis et al. (1992) proposed that the bow-shock structure is due to the interactions of the wind of BZ Cam with the interstellar medium. The wind in BZ Cam was also studied by Honeycutt, Kafka & Robertson (2013). Greiner et al. (2001) suggested that this nebula is photoionized by a bright central object that must be a SSS, while the bow-shock structure is due to the high-proper motion of BZ Cam, moving while it emits the wind.

4.2.1 *X-ray data*

The second plot of Fig. 7 shows the X-ray spectra of BZ Cam observed with the *Swift* XRT. The luminosity is higher in the low state; however, in the very soft spectral region, at energy $\leq$0.5 keV, the X-ray flux is almost twice higher in the high state, which is exactly the opposite of the scenario predicted by Greiner et al. (1999). Interestingly, the spectral fits in both states indicate that we may be observing an unresolved, strong Ne X Lyman α line at 1.02 keV. In the high-state spectrum the Fe XXV line at 6.7 keV is clearly detected. BZ Cam was also previously observed with *ROSAT* in the high state. van Teeseling & Verbunt (1994) and Greiner (1998) fitted the spectrum either with one-component blackbody or with a highly absorbed bremsstrahlung (or MEWE) model. Greiner (1998) favoured the blackbody. However, with the larger energy range of *Swift* we see that a fit including also the high-energy part of the spectrum, is only possible with at least two components, and that the blackbody is not adequate. The black dots in the second panel of Fig. 7 show the low-state spectrum of BZ Cam, and a fit with a two-component VAPEC model. With only a broad-band spectrum and no detected emission lines, we could not adequately fit the cooling flow model. The same is true for other low-resolution X-ray spectra described below.

The high state of BZ Cam (red dots in the second panel of Fig. 7) is best fitted with a two-component VAPEC model. The fitting parameters are listed in Table 5. We find the best fit with non-solar abundances, [Fe/H] = (4.5 $\pm$ 2.4) and [Ne/H] = ($\sim$14). In the low state, the increased flux seems to be due to a higher maximum temperature, 64 keV instead of about 10 keV. The column density N(H) appears to increase in the low state. Again, a lower limit to the blackbody temperature is of about 150 000 K.

4.2.2 *UV observations*

BZ Cam was observed in UV with *Swift* during the low state with a 1172.43 s exposure and with a 121 s exposure during the high state. The UV magnitudes in the AB system in the high and low states, given in Table 6, indicate a smaller variation than observed in the other objects. This is explained by Fig. 8 in which we show the UV image of the nebula obtained with *Swift*/UVOT observations. Even with the poor spatial resolution of UVOT, we detect an extended object; obviously the ionized nebula also emits copious UV flux. Comparing the image of BZ Cam in Fig. 8 and the optical image in fig. 4 of Greiner et al. (2001), we see a trace of the bow shock oriented in the south slightly south-west direction, but there seems to be additional UV emission of the nebula in the north-east direction, unlike in the in O [III] and Hα images taken in September of 2000 with the WIYN telescope (Greiner et al. 2001).

4.3 MV Lyr

MV Lyr spends most of the time in the high state, having brightness in the range $V = 12$–13, and during the occasional short low states it is in the range $V = 16$–18. Historical light curves of MV Lyr can be found in Rosino, Romano & Marziani (1993), Wenzel & Fuhrmann (1983), Andronov & Shugarov (1982) and Pavlenko & Shugarov (1998). With their *FUSE* (*Far Ultraviolet Spectroscopic Explorer*) observations, Hoard et al. (2004) estimated that during the low state $\dot{m} \leq 3 \times 10^{-13}$ M$_\odot$ yr^{-1}, a four orders of magnitude decrease from the value of $\dot{m}$ estimated by Godon & Sion (2011) in the high state.

4.3.1 *X-ray data*

The third plot of Fig. 7 shows the comparison between the high- and low-state X-ray spectra of MV Lyr obtained with *Swift* together

Table 5. Fitting models and parameters for BZ Cam and MV Lyr. The errors represent 90 per cent confidence region for a single parameter.

	BZ Cam			MV Lyr		
	High state		Low state	High state		Low state
Satellite	*Swift*	*Swift*	*Swift*	*Swift*		
Models	VAPEC	2 VAPEC	2 APEC	VAPEC+PLOW	2 APEC	2 APEC
N(H)(10^{22})	$0.14^{+0.03}_{-0.03}$	$0.26^{+0.12}_{-0.08}$	$0.7^{+0.4}_{-0.7}$	$0.24^{+0.5}_{-0.24}$	$0.69^{+0.16}_{-0.26}$	$0.73^{+0.73}_{-0.52}$
Photon Index				$1.00^{+0.5}_{-0.24}$		
T_1 (keV)	$9.3^{+0.2.8}_{-1.7}$	$0.51^{+0.3}_{-0.20}$	$0.3^{+0.0.4}_{-0.3}$	$0.18^{+0.38}_{-0.49}$	$0.11^{+0.03}_{-0.04}$	$0.12^{+0.07}_{-0.05}$
T_2 (keV)		$10.8^{+4}_{-2.3}$	$63.6^{+0.4}_{-54}$		58^{+6}_{-50}	$2.47^{+1.9}_{-1.6}$
Flux$_{\rm abs}$*	$3.85^{+0.24}_{-0.29}$	$4.04^{+0.22}_{-0.3}$	$6.4^{+5}_{-2.2}$	$6.5^{+0.4}_{-1.6}$	$6.0^{+3.5}_{-6}$	$1.2^{+1.3}_{-0.4}$
Flux$_{\rm unabs}$*	$4.24^{+0.24}_{-0.29}$	$4.98^{+0.22}_{-0.3}$	$14^{+5}_{-2.2}$	$9.7^{+0.4}_{-1.6}$	90^{+52}_{-90}	75^{+81}_{-25}
χ^2	1.6	1.1	1.0	1.0	1.2	

*The X-ray flux ($\times 10^{-12}$ erg cm^{-2} s^{-1}) for *Swift* XRT was calculated in the range 0.3–10.0 keV.

Table 6. UV observations.

Object	State	Date	Instrument	Exp.(s)	Mag.$_{AB}$	Filter*
BZ Cam	High	21/12/2012	*Swift* UVOT	1200.74	13.0 ± 1.0	*UVW*2
	Low	15/05/2011	*Swift* UVOT	2737.32	13.198 ± 0.011	*U*
MV Lyr	Low	29/07/2011	*Swift* UVOT	2092.81	16.265 ± 0.019	*U*
TT Ari	High	01/11/2005	*GALEX*	1468.3	12.52 ± 0.001	*FUV*
	High	13/11/2003–03/11/2007	*GALEX*	80–1686	12.518 ± 0.003	*NUV*
	Low	15/11/2009–02/12/2009	*GALEX*	1466–1702	15.364 ± 0.003	*NUV*
	Low	22/11/2009	*Swift* UVOT	6311.28	15.091 ± 0.011	*UVW*2
V794 Aql	Intermediate	15/03/2011	*Swift* UVOT	6186.67	17.073 ± 0.025	*UVW*1
	low	12/07/2011	*Swift* UVOT	4732.45	19.26 ± 0.10	*UVM*2

Swift filters central wavelengths (Å): *U* – 3465, *UVW*1 – 2600, *UVM*2 – 2246, *UVW*2 – 1928.
GALEX UV band (Å): *NUV* – 1750–2800, *FUV* – 1350–1750.

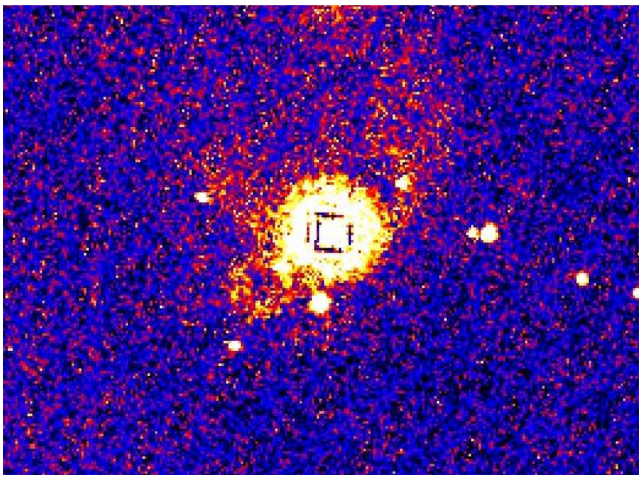

Figure 8. *Swift* UV image of BZ Cam, notice the emission nebula.

with the spectral fits. Unlike in BZ Cam, the high-state X-ray flux of MV Lyr is higher by an order of magnitude than in the low state. The spectrum is also harder, with an additional component prominent above 1.7 keV.

We fitted the high-state spectrum of MV Lyr with a two-component thermal plasma model, but a good fit is also obtained with a thermal plasma and a power-law model. We fitted the low S/N, low-state spectrum with a two-component plasma model with fixed solar abundances, without any attempt to explore the role of the abundances (see Table 5).

A *ROSAT* observation of MV Lyr in 1992 November in the high state was studied by Greiner (1998). The authors fitted the spectrum with a blackbody; however, like in the case of BZ Cam, this model fails to fit the high-energy part of the spectrum that we measured with *Swift*. Greiner (1998) observed MV Lyr at the end of the 9 week optical low state in 1996 and obtained only an upper limit for the X-ray luminosity of $10^{29.7}$ erg s^{-1} assuming a distance of 320 pc (smaller than the most current estimate of 505 ± 50 pc we give in Table 1). Assuming a distance of 320 pc, the flux measured during low-state observation done with *Swift* (see Table 5) four months after the beginning of the decline to the low state, one month after minimum, would be 10^{31} erg s^{-1}, more than a factor of 10 higher than this upper limit. Thus, it seems that the X-ray flux of MV Lyr in the low state is not quite constant.

Table 7. Fitting models and parameters for V794 Aql. The errors represent 90 per cent confidence region for a single parameter.

	High state	Low state
Satellite	*Swift*	*Swift*
Models	2 VAPEC	APEC
N(H)(10^{22})	$0.05^{+0.04}_{-0.03}$	$0.005^{+0.07}_{-0.05}$
T_1 (keV)	$0.9^{+0.3}_{-0.3}$	8^{+20}_{-3}
T_2 (keV)	16^{+39}_{-8}	
Flux$_{\rm abs}$*	$8.2^{+0.5}_{-1.3}$	$2.5^{+0.4}_{-0.6}$
Flux$_{\rm unabs}$*	$8.8^{+0.5}_{-1.3}$	$2.7^{+0.4}_{-0.6}$
χ^2	1.0	0.7

*The X-ray flux ($\times 10^{-12}$ erg cm^{-2} s^{-1}) for *Swift* XRT was calculated in the range 0.3–10.0 keV.

4.4 V794 Aql

In the high-optical state, V794 Aql varies between 14th and 15th magnitude, and in the low states it can plunge to 18–20 mag (in the *B* filter, see Honeycutt & Schlegel 1985). Godon et al. (2007) fitted spectra of the *Hubble Space Telescope* Space Telescope Imaging Spectrograph (*HST*-STIS) and of *FUSE*. They derived the following binary system parameters: $M_{\rm WD} = 0.9\,{\rm M}_\odot$, high state $\dot{M} = 10^{-8.5}$–$10^{-8.0}$ M$_\odot$ yr^{-1}, inclination $i = 60^o$, and distance to the system $d = 690$ pc.

4.4.1 *The X-ray data*

The spectra and their fits of V794 Aql in the intermediate state ($V \simeq 15.5$) and in the low state are presented in the bottom panel of Fig. 7. The X-ray flux is three times higher in the intermediate than in the low state. We fitted the intermediate-state spectrum of V794 Aql with two VAPEC components (see Table 7). In both components, we need high abundance of Mg (∼5). Again, there is no luminous SSS in the low state, with an upper limit of about 150 000 K.

5 DISCUSSION

An important motivation for this research has been the claim by Greiner (1998) and Greiner et al. (2001) that some of the WD in VY Scl-type stars must be burning hydrogen quietly in the low

state, without ever triggering thermonuclear flashes because of the short duration of the burning. We found that the predicted SSS does not appear in the low states, so thermonuclear burning at high temperature is ruled out. However, as we see in Table 1 at least three of the four objects, we investigated have low mass $M_{\rm WD}$. According to Starrfield et al. (2012) thermonuclear burning in WDs whose mass is lower than 1 $M_\odot$ occurs quietly with atmospheric temperature below 150 000 K, outside of the SSS window, except for very high values of the mass accretion rate (see fig. 5 of these authors). For Wolf et al. (2013), we see that WDs with mass up to 0.7 $M_\odot$ burn hydrogen in the stable regime (without nova eruptions) with $\dot{m}$ of a few times 10^{-7} $M_\odot$ yr^{-1} have $T_{\rm eff} \leq 200\,000$ K. We note that also CAL 83, hosting a WD burning H at a much higher atmospheric temperature, has low, intermediate and high states in the optical and X-rays, although with a smaller amplitude in the optical than the VY Scl binaries. These variations were associated with the changes in the amount of irradiation of the accretion disc (see e.g. Greiner & Di Stefano 2002; Rajoelimanana et al. 2013).

All the X-ray spectra of the VY Scl systems we examined appear complex, and the *Chandra* and *Suzaku* spectra of TT Ari clearly indicate more than one emission region or mechanism. The best-fitting model for all the 0.3–10.0 keV broad-band spectra is a, probably still simplistic, two-component absorbed thermal plasma model. Here, we discuss the possible origins of the observed X-ray emission.

5.1 Accretion disc boundary layer

We found that in three of the systems the X-ray luminosity decreases during the optical and UV low states, although the X-ray flux variation is the smallest. The X-ray flux seemed to be anticorrelated with the optical and UV only in BZ Cam. Thus, if in the other three systems the main source of UV/FUV and optical luminosity is the accretion disc, it seems unlikely that the X-ray flux is due to the innermost portion of the disc. In fact, our fits with the cooling flow model, which generally yields good results assuming that all the X-ray flux is emitted in an accretion flow, for all four objects return unreasonably low values of $\dot{m}$, which cannot be reconciled with measurements at other wavelengths. This is not completely unexpected, since the accretion discs of systems accreting at high $\dot{m}$, close to 10^{-8} $M_\odot$ yr^{-1}, seem to re-radiate mostly or completely in the EUV range (Popham & Narayan 1995), because the boundary layer is optically thick.

For TT Ari, the semiregular variability (QPO) with periods of 17–26 min in the high state is best explained with the flickering of an accretion disc; however, we also found that there is no correlation between the X-ray flux and the frequency of the QPO, which would be expected for accretion disc flickering (Baykal et al. 1995; Popham 1999).

5.2 X-ray emission in a wind

If the origin of the X-ray emission is not in the boundary layer of the accretion disc, it may originate in a wind, either from the WD or from the accretion disc, depleting matter from the system. Such a wind may play an important role in the evolution, preventing the WD from reaching the Chandrasekhar mass. The fit of the TT Ari emission lines observed with *Chandra* indicates an FWHM in the range 1100–1500 km s^{-1}. However, the lines do not display any measurable blue or red shift to prove a wind scenario. There is significant broadening, but it may be due to collisional ionization in the accretion flow, or to matter in almost-Keplerian rotation. The WD effective temperature and FUV flux reported in Table 1 are consistent with a line driven wind, although if nuclear burning takes place, the radius of WD at some stage may increase, and we cannot rule out that at some (still not observed) brief stage the WD reaches a luminosity where also electron scattering opacity starts playing a role (a radiation pressure wind like in a nova eruption). In either case, the most likely origin for the X-ray flux in the observations we examined is circumstellar material, shocked when it collides with a new outflow, possibly at a large distance from the WD. There may be circumstellar material left from the AGB phase of primary or old remnant of a previous nova, or a previous 'thicker' wind caused by enhanced luminosity due to nuclear burning, that has slowed down. A strong stellar wind is very likely to play a role in the extended BZ Cam nebula, which was initially classified as a planetary nebula. Instead we would argue that for TT Ari this explanation cannot account for the largest portion of the X-ray flux, because this system shows a 6.4 keV reflection line, which indicates that a large fraction of X-rays (at least X-rays above 7 keV) must originate close to the WD or to the disc.

There is a secure observation of X-rays far away from the accretion disc in UX UMa (see Pratt et al. 2004), an eclipsing NL with a hard, absorbed, eclipsed X-ray component and a soft, unabsorbed, uneclipsed X-ray component. The soft X-rays in UX UMa may indeed originate in a wind from the system. A fast wind is also known to occur in CAL 87 (Greiner et al. 2004; Orio et al. 2004), another system that may be closely related to the VY Scl-type stars. The X-rays and optical flux variations anticorrelate only in BZ Cam, so it is possible that in this system the wind increases in the low state, causing additional absorption and obscuring the accretion disc.

Disc winds are observed in many types of compact objects, while the mechanism that causes them is not completely clear. At optical and UV wavelengths, a mass outflow from the disc has been inferred in some CV via the observation P Cygni profiles, most notably the C IV λ1549 Å line (Robinson 1973; Cordova & Mason 1982; Long & Knigge 2002). P Cygni line profiles or/and absorption features have also been detected in X-rays in low-mass X-ray binaries (Brandt & Schulz 2000; Ueda et al. 2001) and are assumed to originate in a high-velocity outflow from a flared and X-ray-heated accretion disc. Disc winds also cause additional circumstellar, sometimes time-dependent, absorption components in the soft X-rays in non-magnetic CVs (Baskill, Wheatley & Osborne 2001; Saitou et al. 2012).

5.3 Polar caps

A tempting hypothesis is that, while one component of the X-ray flux is due to a mass outflow from the system, another component originates in a different, and coexistent mode of accretion other than the disc, i.e. a stream to the polar caps. In short, the VY Scl would be IPs. This scenario explains the lack of a clear correlation of UV/optical versus X-ray flux variations. As in the model proposed by Hameury & Lasota (2002), the stream to the polar caps still continue, at decreased rate, when the accretion disc is periodically disrupted in the optically low state. In an IP, the disc would emit in optical and UV, but it would be truncated instead of having an X-ray emitting boundary layer, no matter what the value of $\dot{m}$ is.

Mauche (2010) compared spectra of magnetic and non-magnetic CVs and made a point that division into the two classes is not clear-cut on the basis of the X-ray spectrum alone, because of the large variety of observed X-ray spectra of magnetic CVs. There is no 'typical' spectrum among polars and IPs. There is evidence for and

against the magnetic scenario for TT Ari, but the X-ray spectrum alone does not prove or disprove it.

An X-ray flux modulation due to the WD rotation period, which is very typical and is considered the smoking gun to classify IPs, has not been detected in these systems so far. For three of them, the reason may be low inclination, but not so for V794 Aql. However, if the major component of the X-ray flux in the high state is not the accretion stream to the poles, but it is associated instead with a wind, isolating the accretion component for the timing analysis is a serious hurdle in detecting a periodicity due to the WD rotation.

6 CONCLUSIONS

The VY Scl binaries are critical to understand the evolution of WD interacting binaries. They pose several riddles for the theories and understanding them well is a key to a consistent evolutionary picture. Are these systems almost always quietly accreting at a high rate, with short intervals of low $\dot{m}$ that prevent the occurrence of a thermonuclear flash and mass-loss in nova outbursts? Is thermonuclear burning of hydrogen on-going at all phases, and how do we find evidence since we do not observe their WD at the high effective temperature necessary to emit supersoft X-rays?

We analysed a number of X-rays and UV observations of four VY Scl systems comparing phenomena occurring during the optically 'high' and 'low' state. We did not detect supersoft X-ray emission in both states; however, we cannot exclude H burning at a lower temperature, outside of the SSS window, as can be expected from the low masses of the WDs in these systems. The data collected and examined in this paper suggest that the X-ray emission has more than one component in all the four systems. We concluded that one component most likely originates in the circumstellar material, shocked by the wind, possibly at a large distance from the WD while the second component can be X-ray emission from the polar caps. However, we are not able to prove neither clearly disprove an IP scenario for these systems.

It can be argued that the X-ray observations at this stage have posed more new puzzles. We suggest that monitoring these systems over the years in optical, UV and X-rays as frequently and simultaneously as possible is a key to understand how accretion occurs and how it interplays with the thermal state of the secondary. More intensive monitoring, that may be done with *Swift*, would be very rewarding, allowing to understand whether an evolutionary path at high mass transfer rate without mass-loss in nova outbursts can be sustained for a long time, and whether it leads to 'quieter' outflows preventing the WD growth in mass, or to evolution towards a Type Ia supernova.

ACKNOWLEDGEMENTS

Polina Zemko acknowledges the grant of the National Scholarship Programme SAIA and a pre-doctoral grant of the CARIPARO foundation at the University of Padova. Dr Shugarov acknowledges the VEGA grant no. 2/0002/13. We acknowledge with thanks the variable star observations from the AAVSO International Database contributed by observers worldwide and used in this research.

REFERENCES

Andronov I. L., Shugarov S. Y., 1982, Astron. Tsirkulyar, 1218, 3
Andronov I. L., Baklanov A. V., Liakos A., Niarchos P., 2009, Astron. Telegram, 2122
Baskill D. S., Wheatley P. J., Osborne J. P., 2001, MNRAS, 328, 71
Baykal A., Kiziloğlu Ü., 1996, Ap&SS, 246, 29
Baykal A., Esendemir A., Kiziloglu Ü., Alpar M. A., Ögelman H., Ercan N., İkis G., 1995, A&A, 299, 421
Belyakov K. V., Suleimanov V. F., Nikolaeva E. A., Borisov N. V., 2010, in Werner K., Rauch T., eds, AIP Conf. Proc. Vol. 1273, Modeling of the Spectral Energy Distribution of the Cataclysmic Variable TT Ari and Evaluation of the System Parameters. Am. Inst. Phys., New York, p. 342
Brandt W. N., Schulz N. S., 2000, ApJ, 544, L123
Cordova F. A., Mason K. O., 1982, ApJ, 260, 716
Dhillon V. S., 1996, in Evans A., Wood J. H., eds, ASP Conf. Ser. Vol. 208, IAU Colloq. 158: Cataclysmic Variables and Related Objects. Astron. Soc. Pac., San Francisco, p. 3
Ellis G. L., Grayson E. T., Bond H. E., 1984, PASP, 96, 283
Gänsicke B. T., Sion E. M., Beuermann K., Fabian D., Cheng F. H., Krautter J., 1999, A&A, 347, 178
Garnavich P., Szkody P., 1988, PASP, 100, 1522
Godon P., Sion E. M., 2011, PASP, 123, 903
Godon P., Sion E. M., Barrett P., Szkody P., 2007, ApJ, 656, 1092
Greiner J., 1998, A&A, 336, 626
Greiner J., Di Stefano R., 2002, A&A, 387, 944
Greiner J., Teeseling A., 1998, A&A, 339, L21
Greiner J., Tovmassian G. H., di Stefano R., Prestwich A., González-Riestra R., Szentasko L., Chavarría C., 1999, A&A, 343, 183
Greiner J., Iyudin A., Jimenez-Garate M., Burwitz V., Schwarz R., DiStefano R., Schulz N., 2004, Rev. Mex. Astron. Astrofis. Ser. Conf., 20, 18
Greiner J. et al., 2001, A&A, 376, 1031
Greiner J., Schwarz R., Tappert C., Mennickent R. E., Reinsch K., Sala G., 2010, Astron. Nachr., 331, 227
Hameury J.-M., Lasota J., 2002, A&A, 394, 231
Hameury J.-M., Lasota J.-P., Dubus G., 1999, MNRAS, 303, 39
Hessman F. V., 2000, New Astron. Rev., 44, 155
Hoard D. W., Linnell A. P., Szkody P., Fried R. E., Sion E. M., Hubeny I., Wolfe M. A., 2004, ApJ, 604, 346
Hollis J. M., Oliversen R. J., Wagner R. M., Feibelman W. A., 1992, ApJ, 393, 217
Honeycutt R. K., Kafka S., 2004, AJ, 128, 1279
Honeycutt R. K., Robertson J. W., 1998, AJ, 116, 1961
Honeycutt R. K., Schlegel E. M., 1985, PASP, 97, 1189
Honeycutt R. K., Kafka S., Robertson J. W., 2013, AJ, p. 45
Honeycutt R. K., Shears J., Kafka S., Robertson J. W., Henden A. A., 2014, AJ, 147, 105
Hudec R., Huth H., Fuhrmann B., 1984, Observatory, 104, 1
Hudec R. et al., 1987, Ap&SS, 131, 697
Hutchings J. B., Cowley A. P., 2007, AJ, 133, 1204
Kato T., Uemura M., Ishioka R., Nogami D., Kunjaya C., Baba H., Yamaoka H., 2004, PASJ, 56, S1
King A. R., 1997, MNRAS, 288, 16
King A. R., Cannizzo J. K., 1998, ApJ, 499, 348
Krautter J., Radons G., Klaas U., 1987, A&A, 181, 373
Lasota J.-P., 1999, in Mineshige S., Wheeler J. C., eds, Disk Instabilities in Close Binary Systems Disc and Secondary Irradiation in Dwarf and X-ray Novae. Universal Academy Press, Tokyo, p. 191
Leach R., Hessman F. V., King A. R., Stehle R., Mattei J., 1999, MNRAS, 305, 225
Linnell A. P., Szkody P., Gänsicke B., Long K. S., Sion E. M., Hoard D. W., Hubeny I., 2005, ApJ, 624, 923
Livio M., Pringle J. E., 1994, ApJ, 427, 956
Long K. S., Knigge C., 2002, ApJ, 579, 725
Mauche C., 2010, http://cxc.harvard.edu/cdo/accr10/pres/Mauche_Chris.pdf
Mukai K., Kinkhabwala A., Peterson J. R., Kahn S. M., Paerels F., 2003, ApJ, 586, L77
Mukai K., Patterson J., Koff B., Morelle E., Stein W., Oksanen A., 2009, Astron. Telegram, 2254
Mushotzky R. F., Szymkowiak A. E., 1988, in Fabian A. C., ed., NATO ASIC Proc. 229: Cooling Flows in Clusters and Galaxies. Springer, New York, p. 53
Orio M., Ebisawa K., Heise J., Hartmann J., 2004, Rev. Mex. Astron. Astrofis. Ser. Conf., 20, 210

Osaki Y., 2005, Proc. Japan Acad. B, 81, 291
Patterson J., Patino R., Thorstensen J. R., Harvey D., Skillman D. R., Ringwald F. A., 1996, AJ, 111, 2422
Pavlenko E. P., Shugarov S. Y., 1998, Astron. Astrophys. Trans., 15, 89
Pavlenko E. P., Shugarov S. Y., 1999, A&A, 343, 909
Pojmanski G., 1997, Acta Astron., 47, 467
Popham R., 1999, MNRAS, 308, 979
Popham R., Narayan R., 1995, ApJ, 442, 337
Porquet D., Dubau J., 2000, A&AS, 143, 495
Pratt G. W., Mukai K., Hassall B. J. M., Naylor T., Wood J. H., 2004, MNRAS, 348, L49
Rajoelimanana A. F., Charles P. A., Meintjes P. J., Odendaal A., Udalski A., 2013, MNRAS, 432, 2886
Ringwald F. A., Naylor T., 1998, AJ, 115, 286
Robinson E. L., 1973, ApJ, 186, 347
Rosino L., Romano G., Marziani P., 1993, PASP, 105, 51
Saitou K., Tsujimoto M., Ebisawa K., Ishida M., 2012, PASJ, 64, 88
Shafter A. W., Szkody P., Liebert J., Penning W. R., Bond H. E., Grauer A. D., 1985, ApJ, 290, 707
Skillman D. R., Patterson J., Thorstensen J. R., 1995, PASP, 107, 545
Smak J., 1983, ApJ, 272, 234
Starrfield S., Iliadis C., Timmes F. X., Hix W. R., Arnett W. D., Meakin C., Sparks W. M., 2012, Bull. Astron. Soc. India, 40, 419
Thorstensen J. R., Smak J., Hessman F. V., 1985, PASP, 97, 437
Ueda Y., Asai K., Yamaoka K., Dotani T., Inoue H., 2001, ApJ, 556, L87
van Teeseling A., Verbunt F., 1994, A&A, 292, 519
van Teeseling A., Beuermann K., Verbunt F., 1996, A&A, 315, 467
Warner B., 1995, Cataclysmic Variable Stars. Cambridge Univ. Press, Cambridge
Wenzel W., Fuhrmann B., 1983, Mitt. Veraenderliche Sterne, 9, 175
Wolf W. M., Bildsten L., Brooks J., Paxton B., 2013, ApJ, 777, 136
Wu K., Wickramasinghe D. T., Warner B., 1995, PASA, 12, 60

This paper has been typeset from a TEX/LATEX file prepared by the author.